



Research Article

Liquefaction and Reliquefaction Characteristics of Aeolian Sand Foundation Reinforced by Precast Cement Piles Based on Shaking Table Test

Zhaorong Zhu,¹ Yuan Zhou ,² Kan Han,¹ Honggang Wu ,¹ and Shouquan Zhao¹

¹China Northwest Research Institute Co. Ltd. of CREC, Lanzhou, 730070 Gansu, China

²College of Civil Engineering and Architecture, Southwest University of Science and Technology, Mianyang 621000, China

Correspondence should be addressed to Yuan Zhou; 421163324@qq.com

Received 30 August 2022; Accepted 26 October 2022; Published 7 November 2022

Academic Editor: Wensong Wang

Copyright © 2022 Zhaorong Zhu et al. This is an open access article distributed under the Creative Commons Attribution License, which permits unrestricted use, distribution, and reproduction in any medium, provided the original work is properly cited.

With the continuous development of traffic construction, road engineering inevitably crosses the aeolian sand river valley area. Compared with general sandy soil and silty soil, cohesionless aeolian sand foundation has similar properties with fluid and higher liquefaction potential. Precast cement pile can greatly improve the vertical bearing capacity of foundation, but this paper finds that it also has antiliquefaction effect when it is used to reinforce aeolian sand foundation. In addition, there may be more than one liquefaction of aeolian sand foundation in areas with frequent earthquakes. Therefore, this paper explores the liquefaction and reliquefaction characteristics of aeolian sand foundation reinforced by precast cement piles through shaking table test. The test results show that under the excitation of 0.4 g EL Centro wave: (1) the increase of pore pressure in aeolian sand foundation will have multiple instantaneous peaks, which will promote the surface to float or sink. The phenomenon will be weakened by multiple earthquakes or pile reinforcement. (2) The prefabricated cement pile can improve the liquefaction and reliquefaction resistance of aeolian sand foundation. The effect is the best in the shallow layer of the foundation, which is increased by more than 30%, and the deeper the buried depth, the lower the effect. (3) The antiliquefaction ability of foundation will be improved after strong earthquake, but the dynamic response will be significantly increased in the next earthquake. (4) When the aeolian sand foundation reinforced by precast cement piles is reliquefied, the main frequency of the foundation will migrate to low frequency. The liquefied layer will inhibit the low frequency (2 ~ 15 Hz) energy transfer and promote the high frequency (25~30 Hz) energy transfer. The results provide reference for antiliquefaction design of aeolian sand foundation and improve the application of precast cement pile in liquefied foundation.

1. Introduction

Liquefiable sand is widely distributed around the world, and it is inevitable that civil engineering will be built on the sand. When an earthquake occurs, liquefaction will cause surface subsidence, and the effective stress state of the soil will approach 0, causing massive damage to surface structures and underground foundations. Further, with the development of society, people's activity space continues to expand, and some road projects inevitably cross the aeolian sand river-valley area. For example, China's Urumqi-Hami-Lanzhou line, Sichuan-Tibet Railway Lhasa to Linzhi section

and Korla-Golmud line, and other lines of multisegment mileage. Aeolian sand belongs to fine sand with fine particle size and zero cohesion. Aeolian sand is easy to loose and slip under earthquake, and its antiliquefaction ability is weak. In addition, the rich groundwater supplied by the river, frequent strong earthquakes, and the liquefiable nature of aeolian sand make the foundation face the possibility of multiple liquefactions. Precast cement pile is a common foundation treatment method in engineering. Although there is no drainage effect when treating liquefiable foundation, it can greatly enhance the vertical bearing capacity of foundation and share the horizontal load of earthquake.

Therefore, the antiliquefaction effect and reliquefaction resistance of precast cement piles in the treatment of aeolian sand foundation deserve further study.

With abundant groundwater supplied by rivers, frequent strong earthquakes and the easy liquefaction nature of aeolian sand, road foundations face the possibility of multiple liquefaction. In addition, cement-mixing pile is a common foundation treatment method in engineering, and its antiliquefaction effect and reliquefaction resistance in aeolian sand foundation deserve further study. Most studies on sand liquefaction focus on the initial liquefaction. However, earthquakes occur repeatedly in history, and relevant examples show that aftershocks and two strong earthquakes separated by many years can cause liquefaction again [2–4], that is reliquefaction phenomenon. After an earthquake, the density of sand increases with the discharge of pore water and surface subsidence. Olson et al. [5, 6] demonstrated that the reliquefaction resistance will increase accordingly. Based on data compiled by Mesri et al. [7] from ground improvement projects, liquefaction resistance may increase after the relative density increases on the order of 20% to 30%. In addition, even if the sediments have the same initial density, the sand that has undergone preshock has greater stability, which contributes to the improvement of liquefaction resistance [8, 9]. However, some scholars have proposed that the seismic history reduces the reliquefaction resistance of sand despite a significant increase in sand density [10–12]. Ha et al. and Yamada et al. [13, 14] believed that the anisotropy and density of sandy soil jointly affect the reliquefaction phenomenon. When the anisotropy dominates, the liquefaction will be intensified. Otherwise, the reliquefaction resistance will increase. Wang et al. [15] also obtained the same result by numerical DEM test of 2D poly-disperse circular particle material with liquefaction history. Finn et al. [16] concluded that the liquefaction resistance increases if a small shear strain is applied before the cyclic loading test, whereas the liquefaction resistance decreases when the relevant soil is preapplied with a large shear strain. Wang et al. [17] founded that the reconsolidation process after liquefaction of tailings will improve its liquefaction resistance, and proposed that the relationship between the ratio of the cycle number of liquefaction after reconsolidation to the cycle number of first liquefaction and the reconsolidation degree. El-Sekelly et al. and El-Sekelly [18, 19] also found that the previous earthquake history has a significant effect on changing the liquefaction resistance of sandy sediments. His centrifuge experiment results showed that most historical earthquakes can improve the liquefaction resistance of sandy soils, but some larger earthquakes reduce it completely or partially. With the advancement of monitoring technology, scholars have a deeper understanding of the reliquefaction problem at the microscopic level. Ye et al. [20] used a stereo microscope and an industrial camera, combined with digital image processing technology, to obtain meso-parameters indicating that the long-axis direction of the sand particles developed from the horizontal direction in the initial state to the vertical direction after liquefaction, and the reliquefaction resistance decreased. Xie et al. [21] used a microscopic image acquisition system to

observe the changes in the mesostructure of sand bodies under repeated seismic liquefaction events, and concluded that repeated vibrations improved the compactness of sediments, thus increasing the chance of sand grains contacting each other, opening pores, and the generation of elongated pores is less. So, it has a more positive effect on the reliquefaction resistance of sand bodies.

Most of the mentioned literature for foundation liquefaction research are mostly with a certain viscosity of sand and silt as the research object. But, saturated aeolian sand foundation has similar properties to fluid and has higher liquefaction potential. Therefore, it is worth to study the liquefaction characteristics of aeolian sand foundation and explore the reinforcement effect of precast cement pile on this fluid geology. The author made a model of prefabricated cement pile reinforced aeolian sand foundation, using shaking table to simulate the occurrence of earthquake. Based on the macroscopic phenomena and data acquisition results (including surface subsidence, pore water pressure, and acceleration), the liquefaction and reliquefaction characteristics of aeolian sand foundation are analyzed, and the positive role of prefabricated cement piles is explored. The results provide reference for antiliquefaction design of aeolian sand foundation and improve the application of precast cement pile in liquefied foundation.

2. Project Overview

As shown in Figure 1, the satellite image area is located in the Qinghai-Tibet Plateau of China, which belongs to the aeolian sand valley-river area. The river system in this area is developed, the water content of the stratum is high, and the groundwater level is greatly affected by the season. This area is located in the seismic belt of Tibet and Western China, where earthquakes occur frequently and are of large magnitude. The peak acceleration of horizontal ground motions with a probability of exceeding 10% is 0.3 g. Aeolian sand has fine particles, no viscosity, poor water retention, and has strong water sensitivity and dynamic vulnerability. The particle size of aeolian sand is mainly distributed in 0.25 mm~0.074 mm, the maximum dry density is 1.5 g/cm³, and the maximum saturated density is 1.9 g/cm³, and aeolian sand belongs to fine-grained soil sand. According to the exploration data, the thickness of aeolian sand stratum in this area is about 12 m. China's Sichuan-Tibet line Lalin railway passes through the study area, and such landforms are widely distributed in Tibet. China's western transportation construction project will inevitably cross similar landforms. Figure 2 shows the particle size distribution curve of aeolian sand, which includes the sand liquefaction limit proposed by Tsuchida [22], and the aeolian sand is within this range. The foundation filling materials used in the shaking table test in this paper are taken from the original sand on site.

3. Shaking Table Testing Program and Conditions

3.1. Shaking Table and Sensor. This test was carried out in the geotechnical test hall of Southwest Jiaotong University.

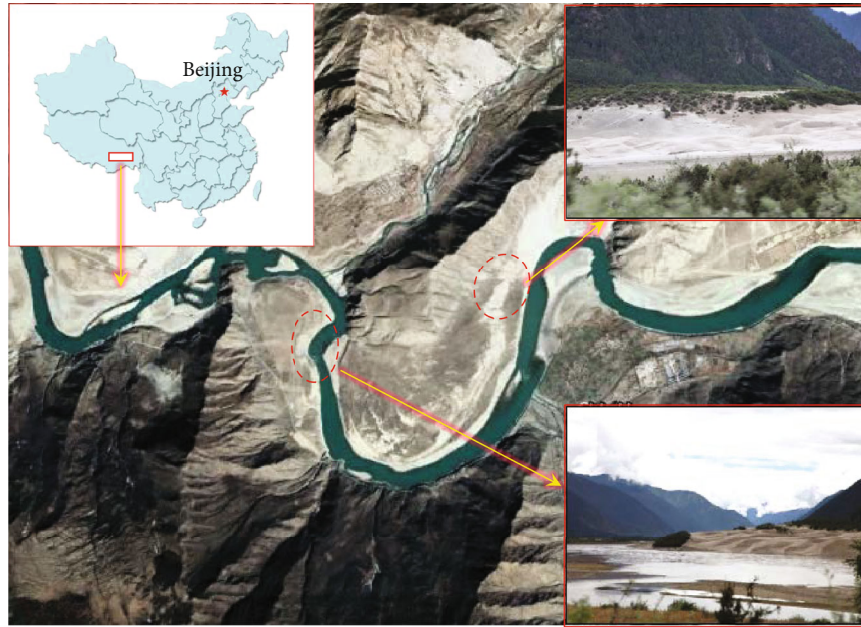


FIGURE 1: Aeolian sand river valley area.

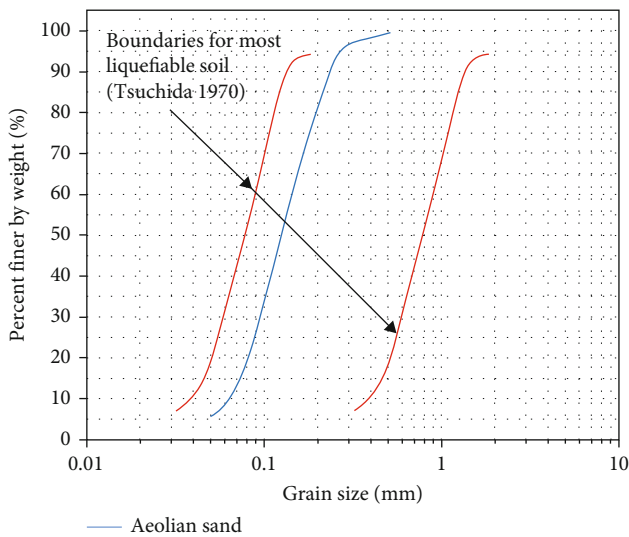


FIGURE 2: Grain size distributions of aeolian sand.

The shaking table and its supporting control system were produced by Suzhou Sushi Testing Group Co., Ltd., model SV-1212. The size of the shaking table was $1.2\text{ m} \times 1.2\text{ m}$, the maximum load is 0.5 t, the working frequency range is 2~1250 Hz, the peak value of horizontal acceleration is 4.37 g, and the maximum displacement is $\pm 51\text{ mm}$. It can output various regular waves, random waves and artificial simulated seismic waves. The test uses a tempered glass model box, the internal size of which is $1\text{ m} \times 0.4\text{ m} \times 0.8\text{ m}$, and the glass side walls are conducive to observing the macroscopic phenomenon of the test. In addition, in order to reduce the influence of reflected waves from rigid walls, a 15 cm foam plate is attached to the side wall of the model box in the vertical excitation direction (2010, 2018) [23, 24]. The foam board is polystyrene foam plastic board, its elastic

modulus is 0.25Mpa, Poisson's ratio is 0.25, ultimate compressive bearing capacity is 75 kPa, density is $14\text{ kg}\cdot\text{m}^{-3}$. Finally, the relevant parameters of the sensor used in this test are shown in Table 1.

3.2. Similarity Ratio Calculation. The purpose of shaking table test is to generate the real response of prototype through scale model. The similarity ratio between prototype and model is worth considering carefully. Limited by the load of the shaking table and the size of the model box, the geometric similarity ratio is 1:20 in this experiment. According to the basis of previous studies [25], this paper selects the geometric size L , the mass density of aeolian sand ρ , the elastic modulus of pile E as the model control variables. This shows that the dynamic duration ratio of model loading is 1:1, because the duration of earthquake without similar ratio compression is better for liquefaction test, otherwise it may lead to no liquefaction of foundation [26]. Its physical quantities are derived from the Buckingham π theorem, as shown in Table 2.

3.3. Test Model Making. Taking the on-site construction of a certain aeolian sand road section as a prototype, precast cement pile has a pile diameter of 2.5 cm, a pile length of 50 cm, and a pile spacing of 6 cm after conversion by similarity ratio. The pile arrangement is a regular triangle. In order to visually compare the liquefaction and reliquefaction characteristics of the aeolian sand foundation strengthened by cement mixing piles, the model box was divided into two halves along the vibration direction to form a piled area and a pileless area. Pore water pressure and acceleration sensors are arranged at different depths of the foundation (Buried depth 10, 30, and 50 cm). The model design and sensor arrangement are shown in Figure 3.

The specific preparation process of the model is as follows: (1) prefabricated cement pile made by PVC pipe,

TABLE 1: Sensor-related parameters.

Accelerometer (model: DH301)		Piezometer (model:CY303)		Laser displacement meter	
Sensitivity(mV/m·s ⁻²)	64.1	Precision	0.1%	Precision	0.05%
Range	±20 m/s ²	Range	0 ~ 50 KPa	Light source	Red laser 670 nm
Frequency range (Hz)	0 ~ 1500			Beam spot size	<0.8 mm

TABLE 2: Similar ratio design for shaking table test.

Physical quantity	Physical symbol	Similarity	Similarity ratio
Geometry	L	S_L	1:20
Mass density	ρ	S_ρ	1
Elastic modulus	E	S_E	1:20
Acceleration	g	$S_g = 1$	1
Linear displacement	s	$S_s = S_L$	1
Self-weight of upper embankment	P	$S_P = S_L^3$	1:20 ³
Dynamic duration	T	$S_T = 1$	1
Pore water pressure	μ	$S_\mu = S_L$	1:20

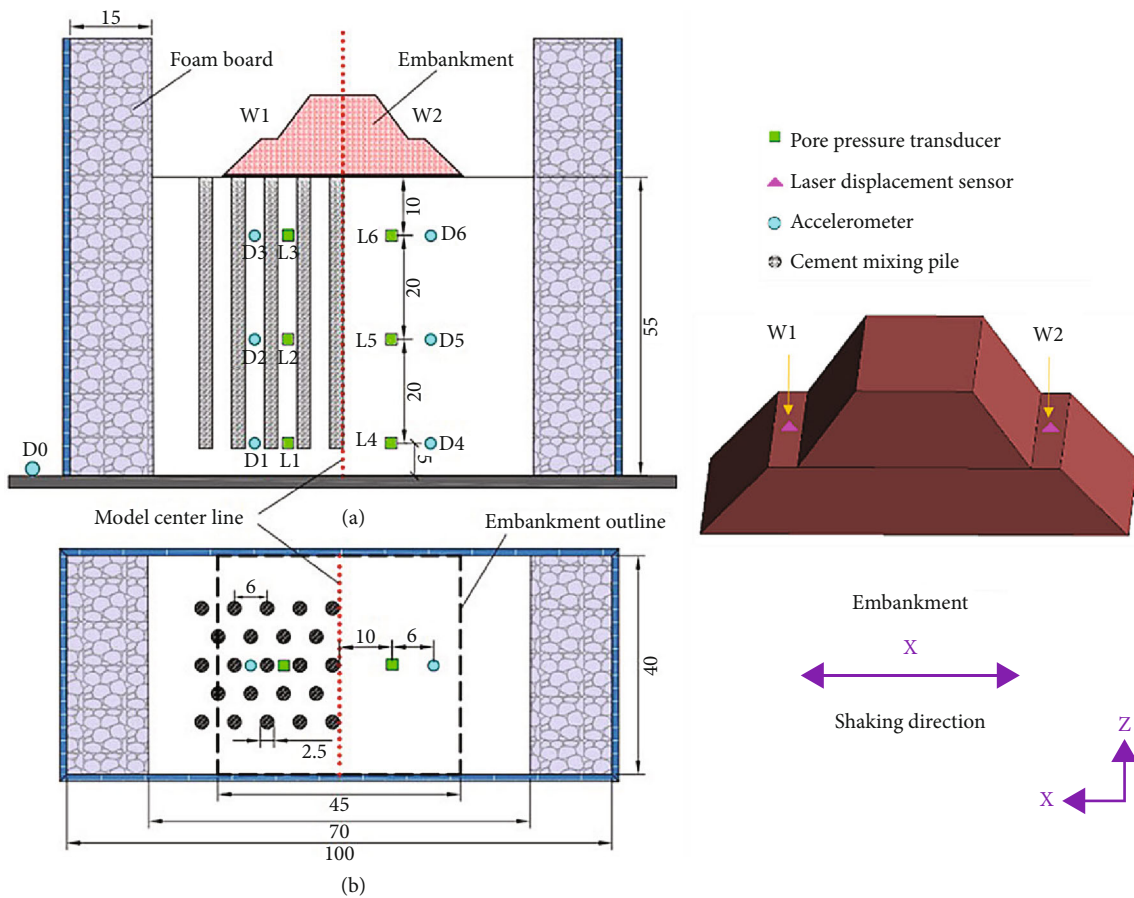


FIGURE 3: Model design and sensor arrangement. (a) Model front view. (b) Model top view.



FIGURE 4: Test details.

pouring at the same time with fine iron bar uniform mixing, and static maintenance of 7 days after removal. (2) The foundation is layered and compacted by hammering. The layered thickness of the foundation filling is 5 cm, and each filling layer is weighed with a ring knife in a total of 4 samples in different regions, and the average density is calculated to control the dry density of the model foundation. During the whole process, the pile is inserted and sensors are arranged. The position of the pile is located by the KT plate with limited holes. (3) After the foundation reaches the target depth, slowly inject water into the model to saturate the foundation. The change of the water level inside the model can be observed through the tempered glass on the side until the water level reaches the surface of the foundation, and the model foundation can be considered to be in a saturated state for 48 hours. (4) Construction of embankments and installation of laser displacement meters. Embankment is made of red clay, only used to simulate the surface load, its mechanical parameters have little effect on the content of this study. In addition, 0.5 cm thick gravel buffer layer exists between embankment and aeolian sand surface. It is worth noting that, in order to prevent the laser of the displacement meter from being affected by the surface water, the displacement measuring points are set on both sides of the embankment. The test details are shown in Figure 4.

3.4. Test Plan. In this test, the earthquake wave was loaded in the X direction, and the waveform was selected from the earthquake waveform widely used by experts and scholars in the field of earthquake research at home and abroad—EL Centro wave. This wave is an earthquake wave with a maximum acceleration of more than 300 gal that was first captured in the United States in 1940 [27], and wave characteristics is shown in Figure 5. It should be pointed out that, since this experiment focuses on the dynamic response between sand and soil-pile systems, combined with the previous research foundation, the use of the original waveform

input has little effect on the research purpose of this experiment, so the seismic wave input has not been processed for similarity ratio [28]. The foundation reliquefaction is studied under the condition of damage accumulation, so by designing the continuous case to induce multiple liquefaction of the foundation, as in the subsequent analysis of the results, case 1 (GK1) is sufficient to induce the first liquefaction event in the model. In subsequent design cases, historical earthquakes, including strong and weak earthquakes, were simulated using multiple earthquake events (during which there was sufficient time to allow water pressure dissipation and consolidation, with intervals of not less than 40 min). The specific loading sequence of seismic waves is shown in Table 3. Since this paper focuses on the comparative study of the liquefaction and reliquefaction, characteristics of precast cement piles strengthens aeolian sand foundation. Therefore, the influence of three strong earthquakes (GK1, GK2, and GK13) on the model is analyzed.

4. Analysis of Test Results

4.1. Macroscopic Phenomenon. Under strong earthquake excitation, the main macroscopic phenomena of the test model are embankment slope settlement, land subsidence, and surface water bursting. Figure 6 shows the macroscopic phenomena of the model under different working conditions. As the figure shows, the unreinforced aeolian sand subgrade was greatly affected by the earthquake. The first strong earthquake (GK1) caused a significant subsidence of the surface of the area, about 3 mm, and a 1 mm water level was formed. After the second strong earthquake (GK2), the subsidence expanded to 5 mm, the water level developed to 2 mm. The third strong earthquake (GK13) only deepened the water level to 3 mm. For the area reinforced by precast cement piles, the ground surface settles by 2 mm only at GK1, and a water level of 1 mm is formed after GK2, while GK13 has no obvious effect on this area. In addition, it can

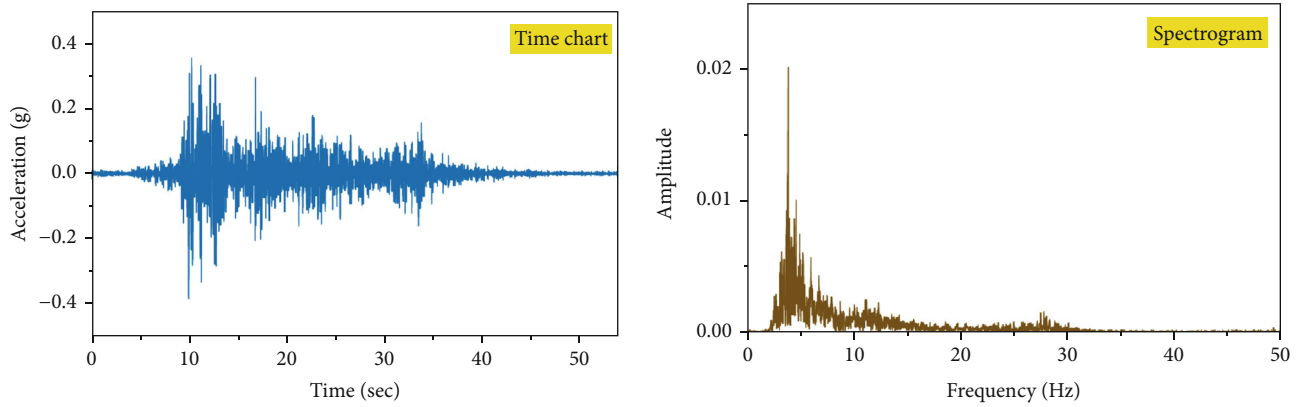


FIGURE 5: Time chart and spectrogram of EL Centro wave acceleration.

TABLE 3: Shaking table loading sequence.

Load order	Peak acceleration/g	Earthquake intensity	Earthquake effects	Type of earthquake waves
GK1	0.4	\geq IX	Strong earthquake: cause foundation liquefaction	EI Centro earthquake waves
GK2	0.4	\geq IX		
GK3	0.3	VII	Weak earthquake: simulation of historical earthquakes between strong earthquakes	
GK4	0.2	VII		
GK5	0.15	VII		
GK6	0.1	VII		
GK7	0.05	<VI		
GK8	0.05	<VI		
GK9	0.1	VII		
GK10	0.15	VII		
GK11	0.2	VII		
GK12	0.3	VII		
GK13	0.4	\geq IX	Strong earthquake: cause foundation liquefaction	

be found that the unreinforced side embankment sinks into the ground, the reinforced side embankment settles synchronously with the ground surface. It shows that precast cement pile can improve the overall stability of aeolian sand foundation. After the test, the model was removed, and it was found that the precast cement pile had no obvious deviation, and the pile body had no cracks and no bending, indicating that the pile was less affected by the earthquake in the liquefiable aeolian sand foundation.

Combined with the settlement curves on both sides of the embankment in Figure 7, the settlement of W2 is significantly higher than that of W1, which is consistent with the macroscopic phenomenon that the embankment is continuously inclined to the unreinforced area under strong earthquakes. In Figure 7, GK1 caused W1 to subside by 2 mm, which is consistent with the surface subsidence in this area. Subsequent earthquakes did not intensify the subsidence of W1, but the settlement curve fluctuated slightly. On the other hand, W2 subsides 4 mm under the action of GK1, and it is worth noting that the curve rises to the peak and then drops instantaneously, indicating that the unreinforced aeolian sand subgrade is more prone to obvious “instantaneous expansion and contraction” phenomenon, resulting

in the embankment rising and falling. Subsidence, W2 also has this feature in GK2, and the subsidence amount reaches 7 mm, and the small fluctuation of the curve reflects the expansion and contraction characteristics of the entire model under the action of earthquake. Under the action of a series of weak earthquake (GK3 ~ GK12), W2 floated up and the subsequent strong earthquake (GK13) caused W2 to sink to 7 mm. Comparing the embankment settlement curve of GK1 and GK2 with the acceleration time history curve, the occurrence of EL Centro wave is first strong and then weak, while the embankment is first sinking and then floating. Compared with GK1 and GK2, GK3 ~ GK12 are a series of weak earthquakes. Therefore, it can be found that strong earthquake tends to shrink the aeolian sand foundation, and weak earthquake tends to expand the aeolian sand foundation. To sum up, the aeolian sand foundation reinforced with precast cement piles has strong ability to resist multiple strong earthquake damage, can effectively restrain the surface subsidence, and prevent the earthquake subsidence of surface structures.

4.2. *Pore Pressure Ratio.* Figure 8 shows the time history of the pore-pressure ratio (excess static pore water pressure/

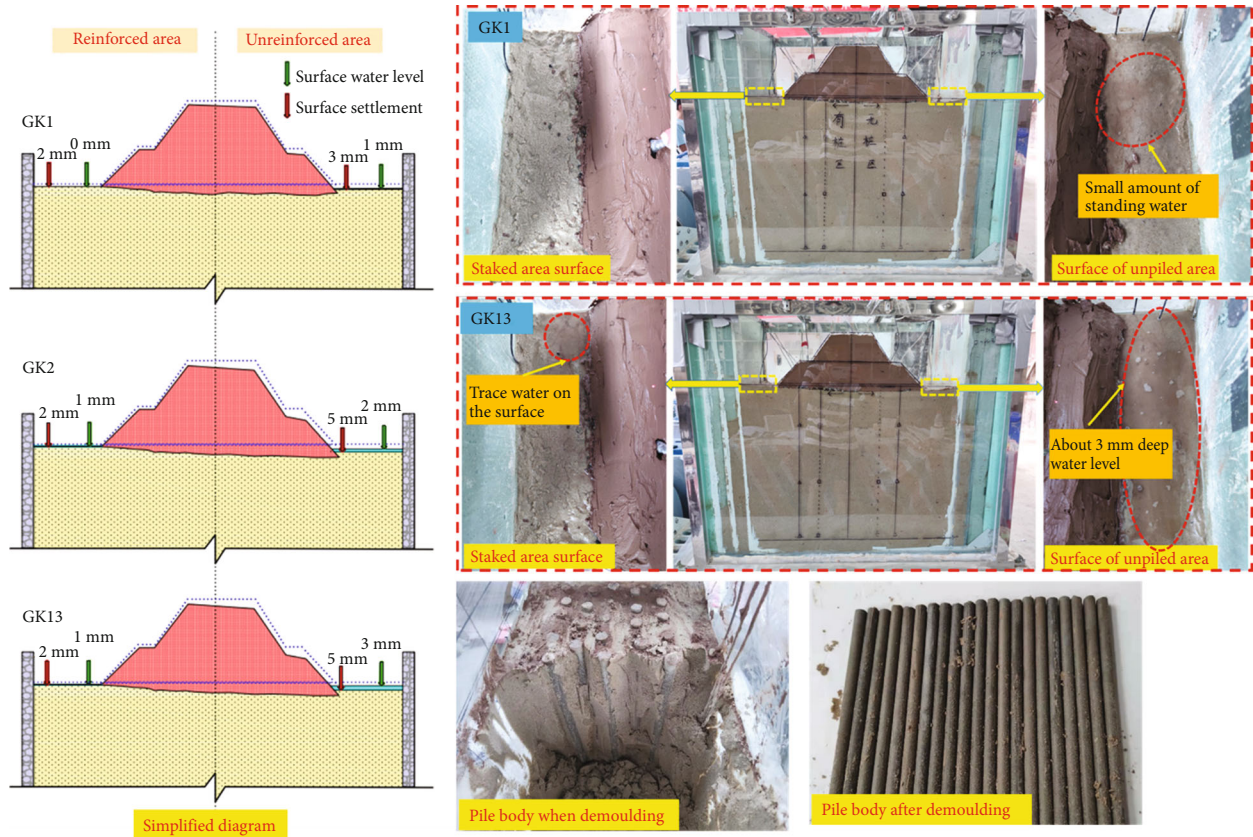


FIGURE 6: Macroscopic phenomena.

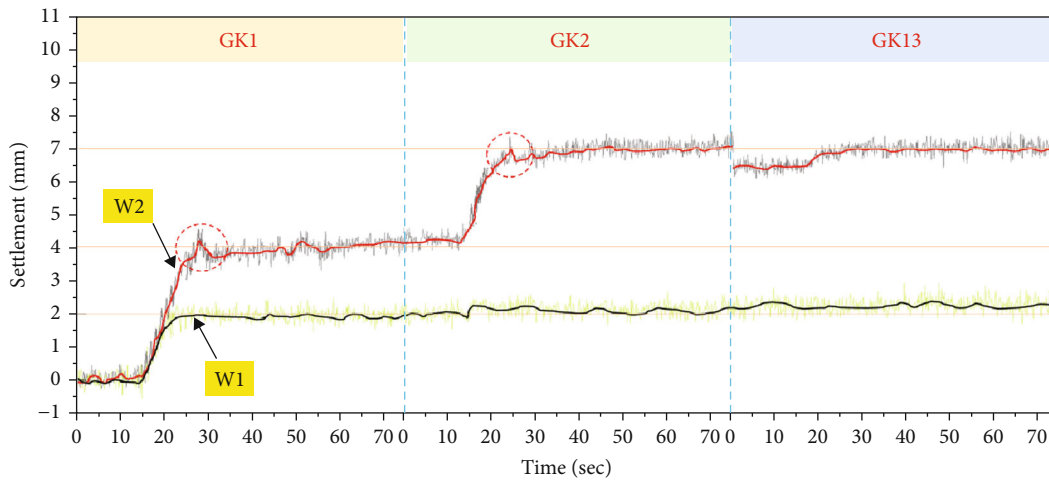


FIGURE 7: Embankment settlement curve.

initial overlying earth pressure) recorded at different depths of the model during the three strong earthquakes. A pore-pressure ratio greater than 1 indicates that liquefaction occurred in this area. In order to illustrate the initial change process of the pore pressure ratio in more detail, the graph is plotted with logarithmic coordinates on the horizontal axis. Two important time periods are marked in the figure, namely the arrival time of liquefaction (the time period during which the pore pressure ratio increases from 0 to 1) and

liquefaction duration (the time period from the first time the pore pressure ratio reaches 1 to the last time it reaches 1). As shown in Figure 8, (1) for the whole model, the growth trend of the pore-pressure ratio is closely related to the buried depth of the measuring point. The fastest growth is at 30 cm, followed by 50 cm, and the growth is not obvious at 10 cm. The corresponding rule is that the middle of the model is the most likely to liquefy, followed by the bottom, and the shallow layers are less affected by the earthquake.

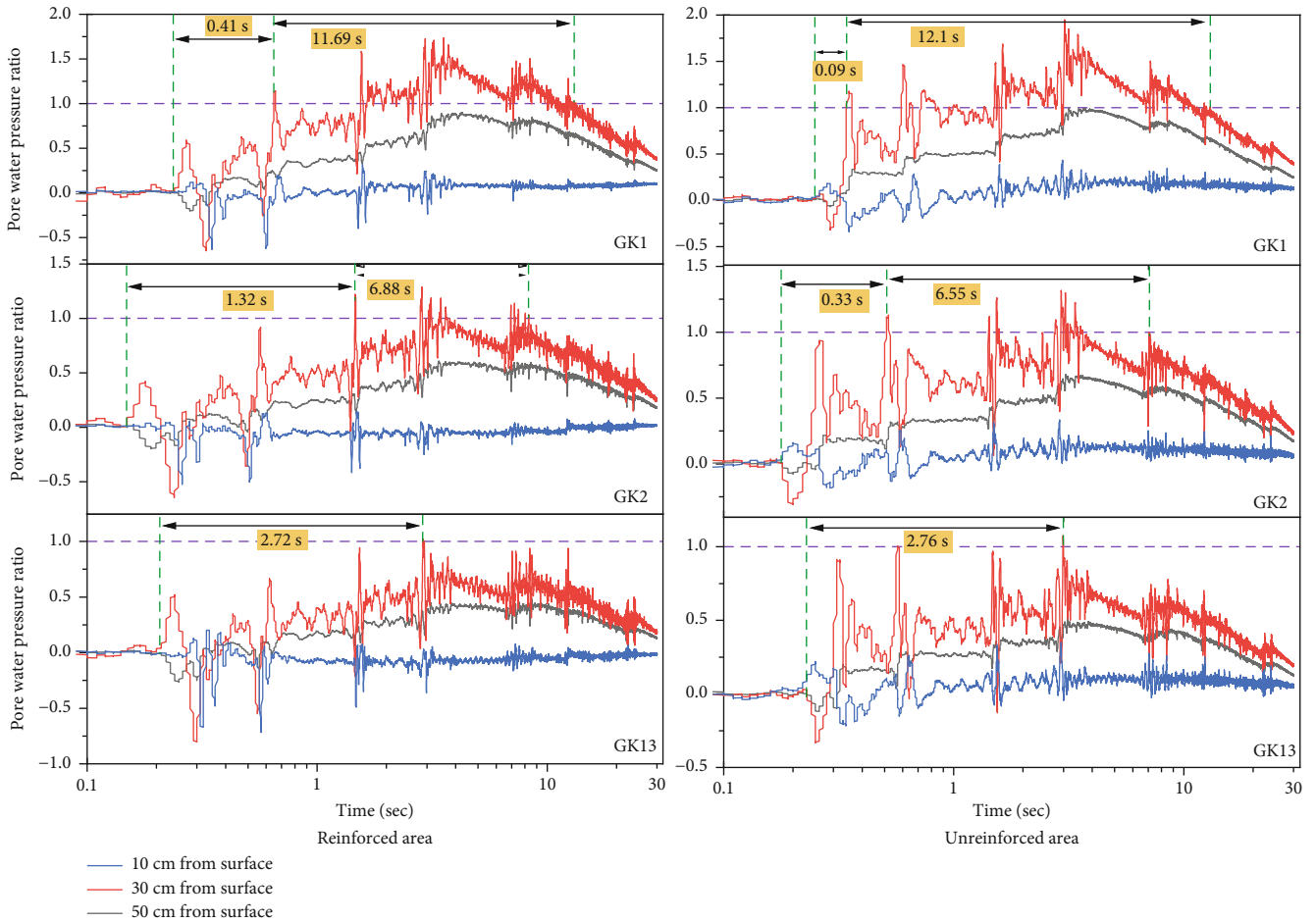


FIGURE 8: Time history curve of pore pressure ratio.

The reason for the results is that the shallow sand is close to the surface, the pore water penetrates to the surface of the foundation faster, and the pore water pressure measured in the deep foundation is large, but the weight of the sand column between the piles is also large, and the corresponding overlying earth pressure value is high, so the pore pressure ratio of the two increases relatively slowly. (2) Focusing on the initial stage of the pore pressure ratio time history curve, there is a phenomenon of “instantaneous negative pore pressure” at each measuring point. The main reason is that due to the “instantaneous expansion” effect of the model when the initial acceleration peak is reached, the pore water pressure meter measures the suction force instead of the pressure instantaneously. So, the instantaneous record of the pore pressure is a negative value. (3) It can be seen from the two important time period changes of the pore-pressure ratio time-history curve at the burial depth of 30 cm; the change rule under the three strong earthquakes is that the first strong earthquake causes the sand layer to reach liquefaction time is short, about 0.41 s, and liquefaction duration up to 11.69 s, but the two subsequent strong earthquakes both prolonged the time to liquefaction and shortened the duration of liquefaction to varying degrees. In addition, pre-cast cement piles in the first two strong earthquakes can effectively prolong the liquefaction time in the middle of

the aeolian sand foundation and reduce the liquefaction duration, but in the third strong earthquake, this advantage is not obvious. (4) Obviously, the pore pressure at the depths of 30 cm and 10 cm does not increase and dissipate regularly under the excitation of 0.4 g EL wave, but has multiple instantaneous peaks. Under the seismic action, the “boiling phenomenon” will occur in the wind-sand foundation, which is described as the expansion and contraction of the foundation at the macroscopic level and the accumulation and dissipation of the super-static pore pressure at the microscopic level.

In order to intuitively reflect the liquefaction and reliquefaction characteristics of different buried depths of the model, the peak pore pressure ratio under three strong earthquakes was plotted according to Figure 8. It can be clearly seen in the figure that the peak pore pressure ratio of all measuring points of GK2 is smaller than that of GK1 from Figure 9.

The results of the third strong earthquake were different. During the GK13, the peaks of L1 and L4 (50 cm buried depth), L2 and L5 (30 cm buried depth) continued to decline, but the observation points L3 and L6 (buried depth 10 cm) have risen. It may be that the surface water level formed and the pore water accumulated in the shallow sandy soil inhibited the dissipation of pore water pressure, resulting in an increase in the peak pore pressure ratio.

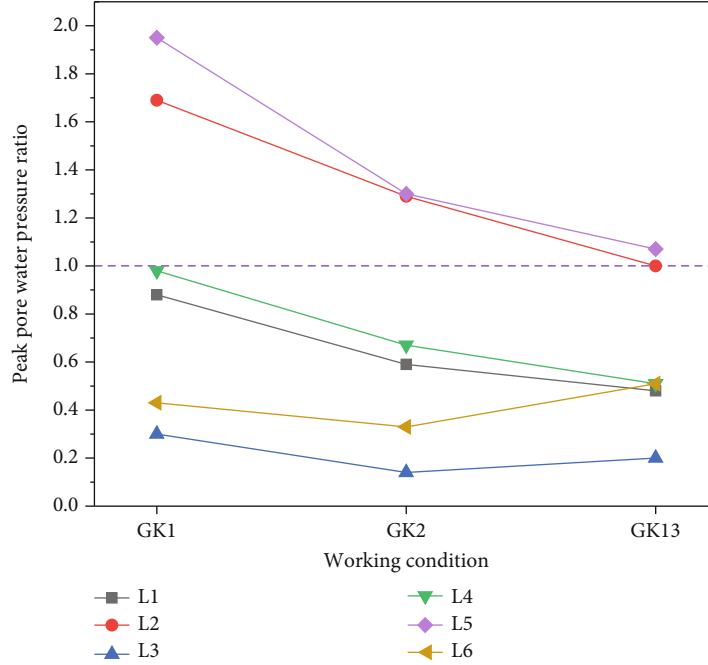


FIGURE 9: Peak curve of pore pressure ratio.

Both the macroscopic phenomenon and the time-history curve of the pore-pressure ratio prove that the precast cement piles can improve the liquefaction resistance of the aeolian sand foundation. In order to quantitatively reflect this capability, based on the peak pore pressure ratio at the same buried depth in the piled area and the unpiled area, the improvement ratio δ of the liquefaction resistance of the cement mixing pile is defined. The formula is as follows:

$$\delta = \left| \frac{v' - v_0}{v_0} \right| \times 100 \frac{0}{0}. \quad (1)$$

In the formula, v_0 is the peak value of the pore pressure ratio in the pile-free area, and v' is the peak value of the pore pressure ratio between the piles at the same burial depth. Figure 10 shows the relationship of δ under three strong earthquakes. As shown in the figure, on the whole, the precast cement piles has the best antiliquefaction effect on the shallow layer of the model foundation, and the value of δ is above 30%, and even reached 57.6% in GK2. The effect of the development of the middle layer of the foundation is greatly weakened, and the effect continues to weaken slightly when it continues to the deep layer. In particular, for GK2, the pile body has the weakest antiliquefaction effect in the middle of the model, where δ is 0.7%, which is equivalent to no pile reinforcement. It may be due to the large subsidence of the surface of the unreinforced area caused by the first strong earthquake, which increased the density of the central part, enhanced the occlusal force between the aeolian sand particles, and formed a more stable structure. Therefore, the liquefaction resistance of the middle of the unreinforced area and the reinforced area are similar. Comparing GK1 to GK13, the delta value of 30 cm buried depth dropped

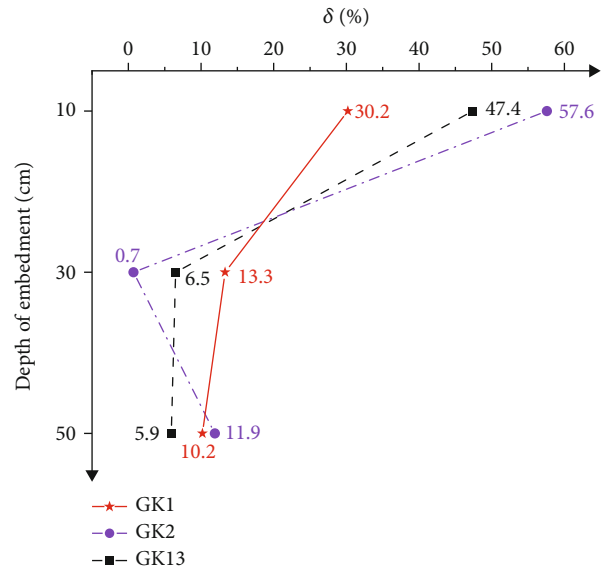


FIGURE 10: Curve of antiliquefaction lifting ratio of cement mixing pile.

from 13.3% to 6.5%, the 50 cm buried δ value dropped from 10.2% to 5.9%, and the shallow buried depth of 12 cm increased from 30.2% to 47.4%. It shows that after several earthquakes, the antiliquefaction ability of precast cement piles will be reduced in the middle and deep foundation of the model, and will be improved in the shallow layer.

Jianning et al. [29] and Tang et al. [30] concluded that the contact surface drainage channel formed by the stone column and the diaphragm wall in the soil under the action of earthquake can promote the release of excess pore water pressure through the pore pressure ratio, indicating that

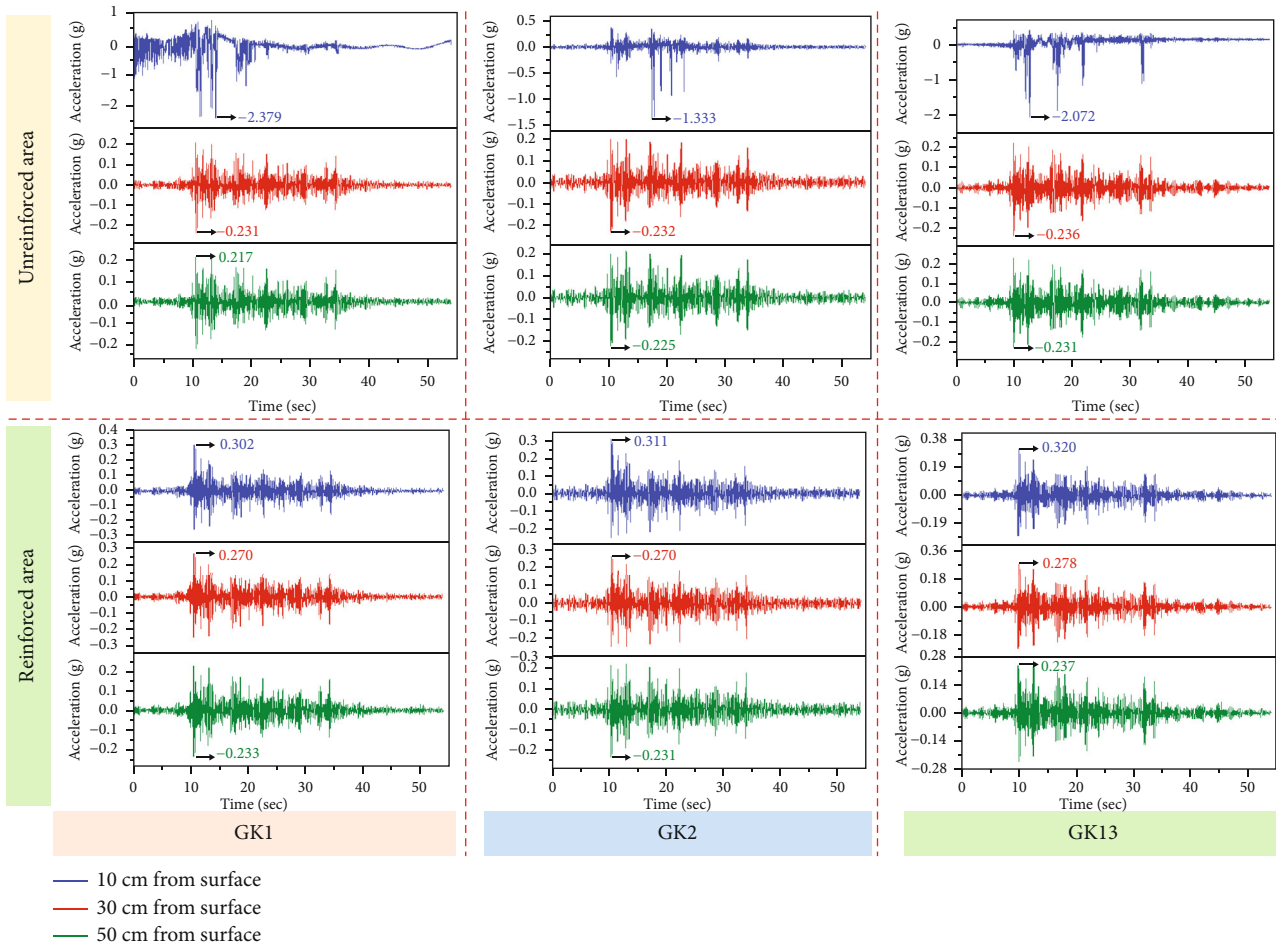


FIGURE 11: Acceleration time-history curve.

the smooth rigid pile has a certain antiliquefaction effect. Therefore, improving the antiliquefaction ability of aeolian sand foundation by precast cement pile can be summarized as two aspects. The first is surface action of pile. Precast cement pile is a smooth rigid pile. Under the action of earthquake, it has a compaction effect on the soil between piles and forms a void surface along the pile body. The pore water of soil between piles seeps to the vicinity of pile surface with vibration, thus enhancing the drainage performance of soil between piles and reducing the accumulation of excess pore pressure. The second is pile action. Since the stiffness of precast cement piles is much greater than that of the interpile soil, most of the shear force caused by the earthquake is borne by the pile body, so the interpile soil stress is relatively reduced. In addition, the presence of the pile restrains the lateral deformation of the soil between the piles and improves the shear strength of the foundation.

4.3. Acceleration Response

4.3.1. Acceleration Time-History Curve Analysis. Figures 11 and 12, respectively, show the acceleration time-history curve and the acceleration peak curve of the measurement points at different buried depths of the model under three strong earthquakes. In Figure 11, in particular, the accelera-

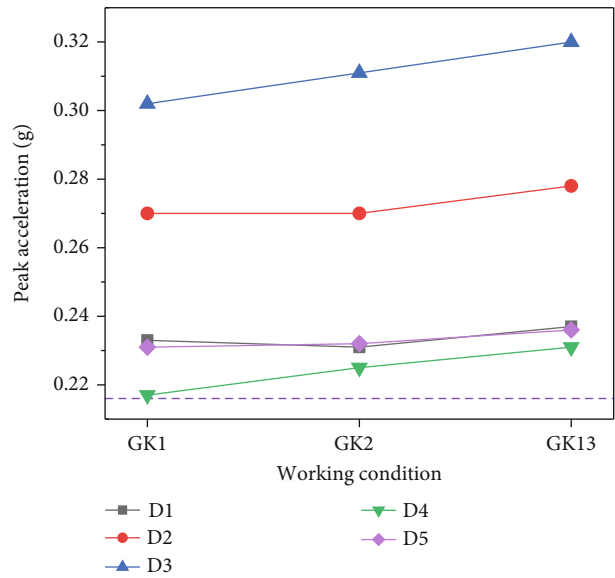


FIGURE 12: Acceleration peak curve.

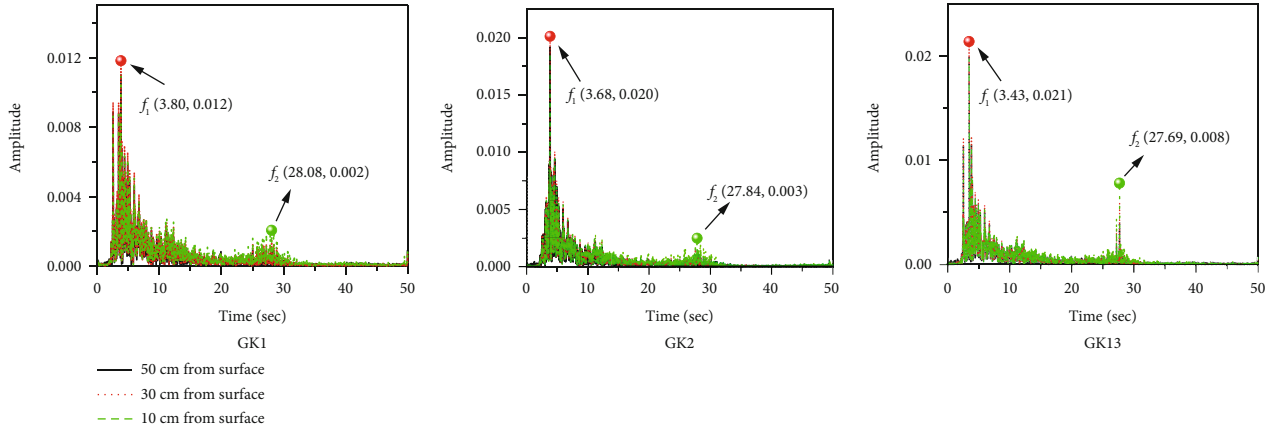


FIGURE 13: Spectrogram.

tion response waveform buried in the shallow layer of the unreinforced area is different from the input wave. This is because the shallow sand is under low overburden pressure and is in a loose state, so it is easy to be disturbed by the earthquake, and the accelerometer data is disturbed during the acquisition. However, it can be found that the waveform of GK2 has a certain stability, because the compactness of this area has been improved after the first strong earthquake, and the data acquisition state tends to be stable.

In Figure 12, the horizontal dotted line is the table acceleration peak line collected when the 0.4 g EL Centro wave is input. The figure shows that the different buried depth measurement points in the model have an amplification effect on the acceleration, and the relationship is proportional to the height of the measurement point from the table. For the same buried depth, the peak value of the acceleration response in the reinforced area is much larger than that in the unreinforced area. It can be seen that the interaction between the pile structure and the aeolian sand foundation has a strong response to the dynamic force. It can be clearly seen that, compared with the previous strong earthquake, the acceleration response peak value of each measuring point of each subsequent strong earthquake has increased.

The mentioned studies show that although the soil layer may have improved liquefaction resistance after undergoing the sand liquefaction process. However, with the improvement of antiliquefaction ability, the dynamic response of soil layer increases significantly in the next earthquake, which may lead to a significant increase in the extent of damage to the foundation and buildings on the surface.

4.3.2. Frequency Response Characteristics. In order to study the frequency response characteristics of aeolian sand foundation strengthened by cement mixing piles under the action of earthquake, the frequency spectrum of each measuring point in the strengthening area was obtained by fast Fourier transform. As shown in Figure 13, in GK1, the frequency components of different burial depths in the reinforcement area are the same, and the energy is mainly concentrated in the low frequency band (2-15 Hz) and the high frequency band (25-30 Hz). There are two excellent frequencies at dif-

ferent measuring points, namely $f_1 = 3.80$ Hz (maximum amplitude is 0.012), $f_2 = 28.08$ Hz (maximum amplitude is 0.002). In GK2, the next two strong earthquakes of the same magnitude almost did not change the frequency spectrum distribution, but the predominant frequency f_1 was reduced to 3.68 Hz, and f_2 was also reduced to 27.84 Hz. Due to the strong seismic excitation of GK1, the foundation subsides, the aeolian sand particles are more closely interlocked, the stiffness of the pile-soil system is improved, and the energy transfer effect of seismic waves from bottom to top is enhanced. Therefore, the maximum amplitudes corresponding to the ground-based excellent frequencies f_1 and f_2 in GK2 have increased. After a series of aftershock history, the ground-based excellent frequencies f_1 and f_2 in GK13 continued to migrate to low frequencies, dropping to 3.43 Hz and 27.69 Hz, respectively, and the corresponding maximum amplitudes continued to increase. It shows that the main frequency of the foundation will migrate to low frequency when reliquefaction occurs after repeated strong earthquakes of the same level after reinforcing the aeolian sand foundation, but the maximum amplitude of the main frequency will increase with different burial depths.

In addition, among GK1, GK2, and GK13, it is remarkable that the measurement point 30 cm above the ground has the largest amplitude at the f_1 frequency, while the measurement point with the largest f_2 frequency response is the measurement point 10 cm above the ground. This is because the liquefaction occurred 30 cm above the ground surface, and the amplitude changes of the energy transmitted by the seismic wave to the shallow layers of the foundation were different in different frequency bands. The specific manifestation is that the liquefied layer inhibits the low-frequency energy transfer, but promotes the high-frequency energy transfer, so the “seismic response elevation amplification effect” of the liquefied foundation still exists.

5. Conclusion

The antiliquefaction (including liquefaction and reliquefaction) effects of precast cement piles reinforced aeolian sand

foundation were evaluated by carrying out the shaking table test under EL Centro wave excitation. The dynamic response law of the foundation under multiple excitations of the same magnitude earthquake is revealed, and the main conclusions are as follows:

- (1) During the earthquake action, due to the multiple instantaneous peaks of pore pressure, the aeolian sand foundation will expand and contract, causing the surface or embankment to float and sink. This phenomenon will be weakened after repeated earthquakes or pile reinforcement
- (2) From the pore-pressure ratio time-history curve, it can be seen that the liquefaction law of the aeolian sand foundation with pile reinforcement and without piles is the same. The middle of the foundation is the most likely to liquefy. The effective stress on the deep layer is the largest, and the liquefaction degree is lower than that in the middle of the foundation. Shallow layer less affected by short drainage path to surface
- (3) The precast cement piles can improve the liquefaction resistance of the aeolian sand foundation. The effect is best in the shallow layer of the foundation, with an increase of more than 30%. The characteristics are greatly weakened in the middle, and slightly weakened in the deep layer. The performance is inversely proportional to the depth of the subgrade
- (4) After the soil layer has undergone the process of sand liquefaction, its resistance to liquefaction will be improved. However, with the improvement of antiliquefaction ability, the dynamic response of soil layer increases significantly in the next earthquake, which may lead to a significant increase in the extent of damage to the foundation and buildings on the surface
- (5) When the aeolian sand foundation reinforced by precast cement piles is reliquefied, the main frequency of the foundation will migrate to low frequency. The liquefied layer will inhibit the low frequency (2~15 Hz) energy transfer and promote the high frequency (25~30 Hz) energy transfer

Data Availability

The basic data of the results of the paper has not been published online, and you can contact the corresponding author at any time to obtain it. Contact email: 421163324@qq.com.

Disclosure

In addition, the manuscript was published as a preprint based on the link: <https://www.researchsquare.com/article/rs-1403356/v1>.

Conflicts of Interest

The authors declare that they have no conflicts of interest.

Acknowledgments

This work was supported by the National Key R&D Program of China (2018YFC1504903) and China Railway Northwest Institute Independent Innovation Fund (XBYKY2018901001).

References

- [1] Y. Zhou, H. Wu, Z. Ma, and H. Sun, "Liquefaction and reliquefaction characteristics of cement mixing pile strengthening aeolian sand subgrade," *researchsquare*, 2022.
- [2] Y. Huang and M. Yu, "Review of soil liquefaction characteristics during major earthquakes of the twenty-first century," *Natural Hazards*, vol. 65, no. 3, pp. 2375–2384, 2013.
- [3] K. Wakamatsu, "Recurrence of liquefaction at the same site induced by the 2011 great East Japan earthquake compared with previous earthquakes," in *Paper Presented at the 15th World Conference on Earthquake Engineering*, Lisbon, Portugal, 2012.
- [4] W. El-Sekelly, R. Dobry, T. Abdoun, and J. H. Steidl, "Two case histories demonstrating the effect of past earthquakes on liquefaction resistance of silty sand," *Journal of Geotechnical and Geoenvironmental Engineering*, vol. 143, no. 6, article 04017009, 2017.
- [5] S. M. Olson, S. F. Obermeier, and T. D. Stark, "Interpretation of penetration resistance for back-analysis at sites of previous liquefaction," *Seismological Research Letters*, vol. 72, no. 1, pp. 46–59, 2001.
- [6] S. M. Olson, R. A. Green, and S. F. Obermeier, "Geotechnical analysis of paleoseismic shaking using liquefaction features: a major updating," *Engineering Geology*, vol. 76, no. 3–4, pp. 235–261, 2005.
- [7] G. Mesri, T. W. Feng, and J. M. Benak, "Postdensification penetration resistance of clean sands," *Journal of Geotechnical Engineering*, vol. 116, no. 7, pp. 1095–1115, 1990.
- [8] D. Su, H. Y. Ming, and X. S. Li, "Effect of shaking strength on the seismic response of liquefiable level ground," *Engineering Geology*, vol. 166, pp. 262–271, 2013.
- [9] J. Teparaksa and J. Koseki, "Effect of past history on liquefaction resistance of level ground in shaking table test," *Geotech Lett*, vol. 8, no. 4, pp. 256–261, 2018.
- [10] S. Wahyudi, J. Koseki, T. Sato, and G. Chiaro, "Multiple-liquefaction behavior of sand in cyclic simple stacked-ring shear tests," *International Journal of Geomechanics*, vol. 16, no. 5, p. C4015001, 2016.
- [11] T. Morimoto, Y. Aoyagi, and J. Koseki, "Effects of induced anisotropy on multiple liquefaction properties of sand with initial static shear," *Soils and Foundations*, vol. 59, no. 5, pp. 1148–1159, 2019.
- [12] H. Iwai, X. Ni, B. Ye, N. Nishimura, and F. Zhang, "A new evaluation index for reliquefaction resistance of Toyoura sand," *Soil Dynamics and Earthquake Engineering*, vol. 136, article 106206, 2020.
- [13] I. S. Ha, S. M. Olson, M. W. Seo, and M. M. Kim, "Evaluation of reliquefaction resistance using shaking table tests," *Soil Dynamics and Earthquake Engineering*, vol. 31, no. 4, pp. 682–691, 2011.

- [14] S. Yamada, T. Takamori, and K. Sato, "Effects on reliquefaction resistance produced by changes in anisotropy during liquefaction," *Soils and Foundations*, vol. 50, no. 1, pp. 9–25, 2010.
- [15] R. Wang, P. Fu, J. M. Zhang, and Y. F. Dafalias, "Fabric characteristics and processes influencing the liquefaction and reliquefaction of sand," *Soil Dynamics and Earthquake Engineering*, vol. 125, article 105720, 2019.
- [16] W. Finn, P. L. Bransby, and D. J. Pickering, "Effect of strain history on liquefaction of sand," *Journal of the Soil Mechanics and Foundations Division*, vol. 96, no. 6, pp. 1917–1934, 1970.
- [17] W. Wang, G. Cao, Y. Li et al., "Experimental study of dynamic characteristics of tailings with different reconsolidation degrees after liquefaction," *Frontiers in Earth Science*, vol. 10, article 876401, 2022.
- [18] W. El-Sekelly, V. Mercado, T. H. Abdoun, R. Dobry, and A. Sepulveda, "Contraction and pore pressure behavior of a silty sand deposit subjected to an extended shaking history," *Soil Dynamics and Earthquake Engineering*, vol. 114, pp. 215–224, 2018.
- [19] W. El-Sekelly, *The Effect of Seismic Preshaking History on the Liquefaction Resistance of Granular Soil Deposits*, [Ph.D. thesis], Rensselaer Polytechnic Institute, Troy, NY, 2014.
- [20] B. Ye, H. Hu, X. Bao, and P. Lu, "Reliquefaction behavior of sand and its mesoscopic mechanism," *Soil Dynamics and Earthquake Engineering*, vol. 114, pp. 12–21, 2018.
- [21] X. Xie, B. Ye, T. Zhao, X. Feng, and F. Zhang, "Changes in sand mesostructure under repeated seismic liquefaction events during centrifuge tests," *Soil Dynamics & Earthquake Engineering*, vol. 150, article 106940, 2021.
- [22] H. Tsuchida, "Prediction and countermeans against the liquefaction in sand deposits," in *Abstract of the Seminar in the Port and Harbor Research Institute*, Yokohama, Japan, 1970.
- [23] J. Chen, X. Shi, and J. Li, "Shaking table test of utility tunnel under non-uniform earthquake wave excitation," *Soil Dynamics and Earthquake Engineering*, vol. 30, no. 11, pp. 1400–1416, 2010.
- [24] Z. Tao, G. Bo, F. Kaixiang et al., "Research on the flexible material of the side wall of the rigid model box under the shaking table test," *Chinese Journal of Rock Mechanics and Engineering*, vol. 37, no. 10, pp. 2415–2424, 2018.
- [25] L. Xianchang, W. Chen, and W. Cheng, "Similar design method of shaking table test model for dynamic interaction of pile-soil-bridge structure in liquefaction site," *Chinese Journal of Rock Mechanics and Engineering*, vol. 3, pp. 450–456, 2004.
- [26] X. Chengshun, D. Pengfei, G. Yancheng, C. Su, and D. Xiuli, "Shaking table test of the influence of the duration compression ratio of ground motion on the seismic response of liquefiable foundations," *Rock and Soil Mechanics*, vol. 40, no. 1, pp. 147–155, 2019.
- [27] T. Ikuo, "Seismic wave propagation in elastic soil with continuous variation of shear modulus in the vertical direction," *Soils and Foundations*, vol. 36, no. 1, pp. 61–72, 1996.
- [28] S. Cesca and F. Grigoli, "Full waveform seismological advances for microseismic monitoring," *Advances in Geophysics*, vol. 56, no. 12, pp. 169–228, 2015.
- [29] W. Jianning, Y. Jing, Z. Haiyang, F. Jisai, and D. Yuanming, "Shaking table test of foundation liquefaction around subway station structure with ground and wall and different spans," *Chinese Journal of Geotechnical Engineering*, vol. 42, no. 10, pp. 1858–1866, 2020.
- [30] L. Tang, S. Liu, X. Ling et al., "Seismic soil liquefaction mitigation using stone columns for pile-supported wharves," *Journal of Earthquake Engineering*, vol. 25, pp. 1–28, 2021.